1

2

Range expansion to record-breaking elevations influences but does not eliminate

***Batrachochytrium dendrobatidis* infections for Andean anurans**

5

6

7 Emma Steigerwald[1,2], Cassandra Gendron[3], Juan C. Chaparro[4], Rosemary G. Gillespie[2], Allie
8 Byrne[1,2], Rasmus Nielsen[5,6,7], Erica Bree Rosenblum[1,2]

9

10

11

12 [1] The Museum of Vertebrate Zoology, The University of California at Berkeley, CA, 94720,
13 USA

14 [2] The Department of Environmental Science, Policy, and Management, The University of
15 California at Berkeley, CA, 94720, USA

16 [3] The Department of Plant and Microbial Biology, The University of California at Berkeley, CA,
17 94720, USA America

18 [4] El Museo de Biodiversidad del Perú, Cusco, Perú

19 [5] The Department of Integrative Biology, The University of California at Berkeley at Berkeley,
20 CA, 94720, USA

21 [6] The Department of Statistics, The University of California at Berkeley at Berkeley, CA, 94720,
22 USA

23 [7] The Globe Institute, The University of Copenhagen, 1350, København K, Denmark

24

25

26

27

28

ABSTRACT

Climate change impacts emerging infectious disease events through multiple mechanisms, but the influence it exerts through driving host range shifts has been little explored. For instance, range shifts may affect pathogen transmission by altering the connectivity of host populations. Additionally, range expanding hosts and pathogens will have different physiological responses to the suites of novel, challenging conditions they are exposed to, influencing infection outcomes. We studied the fungal pathogen *Batrachochytrium dendrobatidis* (*Bd*) on three anuran amphibians in the Cordillera Vilcanota, Peru: *Pleurodema marmoratum*, *Telmatobius marmoratus*, and *Rhinella spinulosa*. There, these species have undergone a climate-driven range expansion into recently deglaciated habitat to become both the highest elevation amphibians and the highest elevation cases of *Bd* infection globally. We analyzed *Bd* genetics, infection metrics, and sublethal impacts along the colonization front (3,900—5,400 m asl) to explore how elevational range expansion affected host-pathogen dynamics. Amphibian range shifts have enabled new connectivity across the once continuously glaciated Cordillera Vilcanota, but genetic evidence suggests that *Bd* disperses so frequently and extensively that this novel connectivity has not contributed significantly to overall *Bd* dispersal. Although amphibians have not escaped *Bd* infection outright through upslope expansion in the Cordillera Vilcanota, *Bd* growth does appear to be constrained at the highest reaches of the Vilcanota. We present evidence that *Bd* infection has different sublethal costs for amphibians at the new elevations they have colonized, but whether the costs are mitigated or exacerbated by extreme elevation may be moderated by amphibian microhabitat use.

52 **KEYWORDS:**

53 *Batrachochytrium dendrobatidis* — climate change— disease triangle — elevational gradient —

54 range expansion—sublethal effects —synergisms — transmission

55

56 **INTRODUCTION**

57

58 The rising incidence of emerging infectious diseases (EIDs) is a critical issue for both

59 conservation and public health (Jones et al. 2008, Fisher et al. 2012). Climate change may be

60 contributing to increased outbreaks by providing pathogens with opportunities to switch hosts,

61 expand geographically, or become more virulent (Harvell et al. 2002, Hoberg and Brooks 2015,

62 Liang and Gong 2017). One little-studied mechanism by which climate change might influence

63 the course of EIDs is by driving hosts to shift their elevational or latitudinal range (Parmesan et

64 al. 1999, Moritz et al. 2008, Freeman et al. 2018). As hosts undergo range shifts, their exposure

65 to novel environments may alter host-pathogen dynamics—potentially exacerbating or

66 mitigating infections, affecting transmission patterns, or exposing hosts to new pathogens.

67

68 The emergence of *Batrachochytrium dendrobatidis* (*Bd*), the fungal pathogen causing

69 chytridiomycosis that has contributed to devastating global amphibian declines (Skerratt et al.

70 2007, Scheele et al. 2019), has been linked to climate change through several hypothesized

71 mechanisms (Li et al. 2013). Climate change may have expanded the geographic extent of

72 optimal *Bd* growth conditions (Bosch et al. 2007). Meanwhile, increased drought frequency

73 compromises amphibian immunity while enhancing *Bd* transmission by causing amphibian

74 aggregation in shrinking water bodies or more humid microhabitats (Burrowes et al. 2004,

75 Lampo et al. 2006). Theory also predicts that increased climatic variability favors rapidly-

76 adapting pathogens over hosts, resulting in faster *Bd* growth and worse infection outcomes (Rohr

77 and Raffel 2010, Raffel et al. 2013). Finally, as parasites generally have broader thermal

78 tolerances than their hosts, frogs are likely to be exposed to suboptimal temperatures before *Bd*

79 is, placing them at a relative fitness disadvantage (Cohen et al. 2017, 2019). The mounting

80 evidence that amphibians are shifting their distributions across the world (e.g. Bustamante et al.

81 2005, Raxworthy et al. 2008, Enriquez-Urzelai et al. 2019) suggests another link between

82 climate change and amphibian-*Bd* dynamics: colonization and exposure to novel environments.

83

84 The Cordillera Vilcanota, in southern Peru, presents an ideal system for exploring how climate-

85 driven range shifts impact EIDs. Field surveys of this heavily glaciated tropical mountain chain

86 in the early 2000s documented the first known *Bd* infections in southern Peru (Seimon et al.

87 2005), but also revealed that three anuran species had expanded their elevational ranges by

88 hundreds of vertical meters into mountain passes that were fully glaciated at the end of the Little

89 Ice Age, only 150 years ago. The Marbled four-eyed frog (*Pleurodema marmoratum*) had

90 expanded upslope to 5,400 m asl, making it the highest elevation amphibian in the world; the

91 Andean toad (*Rhinella spinulosa*) and Marbled water frog (*Telmatobius marmoratus*) had

92 expanded to 5,244 m asl (Seimon et al. 2007). Chytridiomycosis was recorded in *P. marmoratum*

93 and *T. marmoratus* at the upper limits of their distribution, and a die-off event was observed in *T.*

94 *marmoratus* at 5,244 m asl (Seimon et al. 2007). Today, all three anurans persist in the

95 Vilcanota, though at lower abundances, and host-pathogen dynamics have transitioned into a

96 more stable, enzootic state (Seimon et al 2017), as can also be said of neighboring anuran

97 communities downslope (Catenazzi et al. 2017).

98

99   Moving upslope in the Vilcanota, *Bd* and anurans are challenged by increasingly inhospitable

100   conditions: progressively more intense UV radiation, deep frozen precipitation, and a partial

101   oxygen pressure 50-60% of that at sea level (Wang et al. 2014, Poremba et al. 2015, Seimon et

102   al. 2017). At the apex of the Vilcanota mountain passes, soil temperature can dip to –12°C at

103   night and reach 25°C during the day, with a soil freezing rate exceeding that measured from any

104   site on Earth ($1.8°C\ h^{-1}$; Schmidt et al. 2009). Resident frogs can be exposed to an even broader

105   operative temperature range (−3.5 to 44°C; Reider 2018). Here, we ask how range expansion

106   upslope to these new, challenging elevations may have influenced frog-*Bd* infection dynamics.

107   We used genetic data to inform our understanding of the local history of *Bd*, then examined site-

108   level infection metrics and sublethal infection impacts to understand how conditions at newly-

109   colonized elevations might sway infection outcomes. We anticipate that *Bd* in the Vilcanota is

110   from the global panzootic lineage (*Bd*GPL), the lineage largely responsible for *Bd* epizootics in

111   South America (James et al. 2015), though these highest elevations inhabited by *Bd* presumably

112   impose strong selective pressures that could conceivably result in the evolution of a locally-

113   adapted *Bd*GPL strain. If *Bd* remains dispersive despite extreme high-elevation conditions, and

114   particularly if it was introduced to the Vilcanota just before die-offs occurred there in the early

115   2000s, *Bd* will be spatially unstructured, a common finding elsewhere *Bd* population genetics

116   have been studied (e.g. Byrne et al. 2019, Alvarado-Rybak et al. 2021, Basanta et al. 2021).

117   However, if *Bd* persistence in the environment is depressed by harsh, high elevation conditions,

118   the genetic structure of *Bd* may reflect its gradual spread between watersheds by way of anuran

119   dispersal along the deglaciated corridors provided by mountain passes (Haddad et al. 2014). The

120   present study is the first to examine site-level *Bd* metrics above 4000m asl; though *Bd* infection

121 prevalence and intensity tend to initially increase with elevation, studies sampling to 4000 m asl

122 suggest that these metrics may decline with increasing elevations at the range we sampled here

123 (3,900—5,400 m asl; Muths et al. 2008, Catenazzi et al. 2011). For this reason, we expect *Bd*

124 infection to have lower sublethal impacts for amphibians at newly-colonized, extreme high

125 elevation sites. Alternatively, if the stress of high elevations and *Bd* infection impact amphibians

126 synergistically, the sublethal impacts of *Bd* may increase with increasing elevations. These

127 analyses provide the first insights into how the contemporary, climate-change-driven range shifts

128 of hosts may influence EID events.

129

MATERIALS AND METHODS

131 **Fieldwork**

132

133 The Cordillera Vilcanota (13.74°S, 71.09°W) is an 80 km-long mountain chain in the southern

134 Peruvian Andes, crossing the departments of Cusco and Puno. We sampled *P. marmoratum*, *R.*

135 *spinulosa,* and *T. marmoratus* during the transition between the wet and dry seasons (March-

136 May) in 2018 and 2019. Whereas *T. marmoratus* breed throughout the year, *P. marmoratum* and

137 *R. spinulosa* are in their final months of reproductive activity at this time, such that tadpoles can

138 be sampled even when adults are difficult to locate. We sampled at 76 sites across three

139 watersheds: the Alto Urubamba on the interandean versant and the the Inambari and Yavero on

140 the Amazonian versant. Sites ranged from 3,967—5,333 m asl, including transects across two

141 deglaciated passes (Fig. 1). We spent approximately equal person-hours at each sampling site,

142 capturing tadpoles by scoop net and searching for post-metamorphic stages under rocks and

143 along the edges of water bodies. We attempted to capture 15 adults per species per site. If we

144 could not locate 15 adults, we supplemented first with juveniles and then with tadpoles. We

145 sampled 695 *P. marmoratum* (317 adults), 173 *Rhinella spinulosa* (82 adults)*, and 232 *T.

146 marmoratus* (23 adults).

147

148 Post-metamorphic individuals were dry swabbed 7X along the ventral surface of each limb and

149 the vascular patch to assess *Bd* infection; tadpole mouthparts were swabbed 25X (MW113,

150 Medical Wire & Equipment Co., Ltd., Corsham, Wiltshire, UK; Boyle et al. 2007). Swabs were

151 air dried and stored dry or in 80% ethanol. We collected 30 paired dry- and ethanol-stored swabs

152 to compare their efficacy in preserving *Bd* DNA. We noted snout-vent length (SVL), mass, sex,

153 and signs of disease in adults (lethargy, excessive sloughing, reddened skin). Individuals with

154 nuptial pads were considered adult males. Adult male SVL were used to derive a lower-end size

155 threshold for classifying adults, since males of these species are smaller than females: 19mm for

156 *P. marmoratum*; 30mm for *R. spinulosa*; and 29mm for *T. marmoratus*. Post-metamorphic

157 individuals without nuptial pads that exceeded this threshold were classed as adult females. We

158 also recorded SVL, mass, and signs of disease in juveniles; as well as SVL, mass, and Gosner

159 developmental stage (Gosner 1960) in tadpoles. Samples were transported to the University of

160 California, Berkeley for -80°C storage.

161

162 DS1921G Thermocron Temperature Loggers (OnSolution Pty Ltd, Sydney, Australia; hereafter,

163 'iButtons') were placed at a subset of 20 sampling sites during the 2018 sampling season, with

164 paired iButtons deployed to measure temperature every four hours in either aquatic or terrestrial

165 microhabitats. Aquatic iButtons were protected with rubber spray sealant, glued to the inside of a

166 3cm-diameter PVC tube of 12cm length, and placed in ephemeral ponds containing *P.*

167 *marmoratum* tadpoles. Terrestrial iButtons were glued to the inside of a 10cm funnel, which was

168 placed upside down and covered with rocks in location where adult *P. marmoratum* occurred. Data

169 was downloaded from recovered iButtons during the 2019 sampling season.

170

171 **Bd quantification and genotyping**

172

173 We focused on gaining a comprehensive understanding of Bd dynamics in our most widely-

174 sampled anuran, *P. marmoratum.* We estimated *Bd* zoospore equivalents (ZE) per swab using

175 triplicate quantitative PCR reactions (Hyatt et al. 2007; see Supporting information for details).

176 Amplicon sequencing libraries were prepared for 96 *Bd+* extracts on a Fluidigm Access Array

177 and sequenced with Illumina Miseq (Byrne et al. 2017). We processed sequences with the

178 reduce_amplicons.R script (https://github.com/msettles/dbcAmplicons) and produced BAM files

179 and ambiguity sequences as substrates for the following analyses (see Supporting information for

180 details).

181

182 **Phylogenetic, structure, and redundancy analyses**

183

184 We processed ambiguity sequences separately for Vilcanota samples and a larger dataset that

185 included previously published genotypes representative of global *Bd* diversity (Byrne et al.

186 2019). In R, we removed one sample for each of six amplicons that resulted in >5bp length

187 differences, samples with >80% missing amplicons, and amplicons with >33.3% missing

188 samples. We aligned filtered ambiguity sequences in MUSCLE (v3.32; Edgar 2004). In

189   Geneious (v2021.1.1), we checked for alignment issues and estimated a ML gene tree for each

190   amplicon using RAxML (v4.0) with the GTR substitution model and the rapid bootstrapping

191   method for 100 bootstraps. We collapsed gene trees in Newick Utils (v. 1.6) by branches with

192   <10 bootstrap support to improve tree accuracy, then estimated an unrooted species tree in

193   ASTRAL (v5.7.4) and visualized in GGTREE (v3.0.2).

194

195   To examine standing genetic variation of Vilcanota *Bd*, we used BAM files to create a Site

196   Frequency Spectrum (SFS) in ANGSD (v0.933-106-gb0d8011). BAMs were then processed

197   separately for the subset of Vilcanota samples retained in phylogenetic analyses and the larger

198   dataset including globally representative *Bd*GPL samples (Byrne et al. 2019). We indexed BAMs

199   in SAMtools (v1.11) and detected variants with a minimum coverage of 10X in FreeBayes

200   (v1.3.2-46-g2c1e395). We conducted a principal component analysis with a NIPALS PCA based

201   on an ANGSD covariance matrix (Korneliussen et al. 2014), a method only evaluating pairwise

202   sets of individuals at loci for which they are both sequenced. We tested for population structure

203   at the scale of sampling sites and watersheds, using a pegas-based, clone-corrected AMOVA in

204   Poppr (Kamvar et al. 2014). We also assessed the proportion of genetic variance that could be

205   explained by elevation in R by imputing missing genotypes with the random-forest method

206   MissForest (v1.4), conducting a redundancy analysis in Vegan (v2.5-7), and calculating the

207   adjusted r^2 value and predictor p-values of the resulting model with ANOVA in Stats (v4.1.1).

208

209   **Infection dynamics across elevations**

210

211   We analyzed the site-level effects and sublethal impacts of *Bd* in R (v4.0.2; see Supporting

212   information for details). First, we used GLMs to examine the influence of elevation on

213   population density— based on adults for *Pleurodema marmoratum* and *Rhinella spinulosa* and

214   all life stages for the endangered *Telmatobius marmoratus*—in MASS (v7.3-54). We investigated

215   whether elevation predicted site mean infection intensity, maximal infection intensity, or

216   prevalence through linear and quadratic regression models. Finally, we examined whether frog

217   body size (SVL) and condition (SMI, as per Peig and Green 2009) responded to site infection

218   status, elevation, and site as a random effect for *P. marmoratum* adults, *P. marmoratum* tadpoles,

219   and *T. marmoratus* tadpoles using GLMMs in lme4, omitting the remaining species-life stage

220   combinations due to insufficient sample sizes. We included Gosner developmental stage as a

221   partial correlate predicting tadpole SVLs. To explore how thermal regimes along the elevational

222   gradient might relate to observed trends in infection metrics and sublethal impacts, we plotted

223   March-April temperature data from recovered iButtons relative to the temperature-dependent

224   logistic growth rate (r) of a tropical *Bd* strain (Voyles et al. 2017), the CT_{max} of adult *P.*

225   *marmoratum*, and the mean temperature tolerated by *P. marmoratum* adults that recovered

226   following freezing (Reider et al. 2020).

227   **RESULTS**

228

229   **Phylogenetic placement, spatial genetic structure, and local adaptation**

230

231   *Bd* samples from *P. marmoratum* in the Vilcanota ($n = 44$) nest phylogenetically within the

232   *Bd*GPL-2 clade of the *Bd*GPL lineage. *Bd* samples did not form a clearly-differentiated strain

233 (Fig. 2, Fig. S1), as was also evident in a PCA of globally-derived *Bd*GPL genotypes (Fig. 3A).

234 *Bd* from the Vilcanota is locally unstructured, with samples failing to cluster geographically in a

235 PCA or consensus gene tree (Fig. 3B, Fig. S2), despite containing many low-frequency variants

236 that were robust to stringent filtering (73.4% variants have an allele frequency of ~1%). No clear

237 differentiation of watersheds or sites was evident in an AMOVA ($p > 0.05$, Table S1).

238 Redundancy analysis identified elevation as a significant predictor, though only explaining 1.2%,

239 of genetic variance ($p < 0.05$, Table S2).

240

241 **Site infection metrics across elevations**

242

243 We recorded adult *Pleurodema marmoratum* and *Telmatobius marmoratus* at the core of Osjollo

244 Pass, at a maximal elevation of 5,333 and 5,226 m asl respectively. We sampled *P. marmoratus*

245 at regular intervals across the entirety of both Osjollo and Chimboya Passes, suggesting that

246 these deglaciated passes now provide new connectivity between populations north and south of

247 the Vilcanota. Our proxy of population density in *P. marmoratum* ($n_{sites} = 63$) and *T. marmoratus*

248 ($n_{sites} = 17$) did not correlate with elevation (Fig. S3A-B). We detected *R. spinulosa* only up to

249 4,895 m asl, and adult counts of *R. spinulosa* declined by 6.4 animals per 1000m increase in

250 elevation ($n_{sites} = 25$, $p < 0.001$, Fig. S3C, Table S3).

251

252 *Bd* prevalence in *P. marmoratum* was 30.0% among juveniles ($n = 120$) and 24.0% among adults

253 ($n = 317$), but not detected in tadpoles (n = 256). The best model by AIC relating elevation to *Bd*

254 prevalence was a quadratic model, with *Bd* prevalence peaking midway along the high elevation

255 gradient (approx. 4700 m.a.s.l; Fig. S4A, Table S4). The predictors in this model were

256   significant and explained 20% of variance in prevalence (n_{sites} = 18, $p < 0.05$, Table S4). Visual

257   inspection of plots of infection intensity against elevation suggested that these metrics declined

258   with increasing elevation (Fig. S4B-C), but data supported neither a linear nor a quadratic

259   relationship between site mean or maximal infection intensity and elevation (n_{sites} = 18).

260

261   **Sublethal impacts across elevations**

262

263   In *Telmatobius marmoratus* tadpoles, a full interactive model including elevation and site

264   infection status as predictors of body condition (SMI) minimized AIC and explained 11% of

265   variance in the data (n = 77, n_{sites} = 6, Table S5), though this model may be overfit. All predictors

266   were significant ($p < 0.05$), except the slope of SMI against elevation at *Bd+* sites. This model

267   suggests that tadpoles attained higher body conditions at lower elevations at *Bd-* sites, but did not

268   experience this energetic benefit at low elevations at *Bd+* sites (Fig. 4A).

269

270   Similarly, *T. marmoratus* tadpole body size (SVL) was best predicted by a full interactive model

271   that included elevation, site status, and developmental stage as a partial correlate. All predictors

272   were significant, with fixed effects explaining 68% of the variance (n = 77, n_{sites} = 6, $p < 0.001$,

273   Table S6). Consistent with our findings regarding *T. marmoratus* tadpole SMI, the best-fit model

274   suggested that tadpoles are longer relative to developmental stage at lower elevations, but only at

275   *Bd-* sites (Fig. 4B).

276

277   The model predicting *P. marmoratum* tadpole SMI from elevation and site status with lowest

278   AIC included elevation only. According to this model, body condition declined with increasing

279 elevation, but the model predictors were not significant, and the fixed effects explained only 4%

280 of variance in SMI ($n = 128$, $n_{sites} = 15$, $p > 0.05$, Table S5). Visual inspection of these data

281 revealed that SMI appeared reduced for lower elevation tadpoles at $Bd+$ sites, similar to trends

282 detected for *T. marmoratus* tadpoles (compare Fig. 4A and Fig. S5C). Indeed, a model including

283 site status and its interaction with elevation was within a ΔAIC of only 0.02 of the elevation-only

284 model, explained 7% of variance in SMI, and included a significant slope and intercept at Bd-

285 sites (Table S5). Meanwhile, *Pleurodema marmoratum* tadpole SVL was best predicted by

286 elevation alone. Tadpoles were longer relative to developmental stage at higher elevations

287 regardless of site infection status (Fig. S6A). The model explained 18% of variance in SVL, but

288 not all predictors were significant ($n = 128$, $n_{sites} = 15$, $p > 0.05$, Table S6).

289

290 In *P. marmoratum* adults, the best model of SMI by AIC was an additive model that included

291 elevation and site infection status, though these predictors were not significant and explained

292 only 3% of variance in SMI ($n = 339$, $n_{sites} = 53$, $p > 0.05$, Table S5). Based on this model, adults

293 had lower body conditions at high than at low elevations, and at $Bd+$ than at Bd- sites. Visual

294 inspection of these data reflects the trends that emerged for *T. marmoratus* tadpoles (compare

295 Fig. 4A and Fig. S5B): SMI was depressed for lower elevation tadpoles at $Bd+$ sites. However,

296 the full interactive model was not well supported by AIC-based model comparison (Table S5).

297

298 In adult *P. marmoratum*, SVL was best predicted from a full interactive model of elevation and

299 site *Bd* infection status. Fixed effects in this model explained 9% of variance in SVL, but though

300 all the predictors were significant the intercept was not ($n = 339$, $n_{sites} = 53$, $p > 0.05$, Table S6).

301 According to this model, SVL in adult *P. marmoratum* increases with increasing elevation,

302 regardless of site infection status. However, while SVL increases rapidly at *Bd-* sites (6.5mm per

303 1,000m of elevation), SVL increases only gradually at *Bd+* sites (1.4 mm per 1,000m; Fig. S6B).

304

305 Temperature data from iButtons along the elevational gradient demonstrated that higher

306 elevations were characterized by lower average daily temperatures and larger fluctuations in

307 daily temperature (Fig. 5A). Ephemeral pond habitats, as expected, experienced less thermal

308 variability than adjacent terrestrial habitats (Fig. 5A). It follows that, at higher elevations, *Bd* is

309 characterized by a lower average rate, but anurans also experience greater exposure to their

310 physiological tolerance limits (Fig. 5B).

311

312 **DISCUSSION**

313

314 Understanding how climate change and novel pathogens interact to challenge wildlife is of

315 critical concern to conservation and public health, but we know little about how host range shifts

316 driven by climate change may impact infection dynamics. We used genetic analyses and

317 modeled the relationship among elevation, site infection metrics, and the sublethal impacts of

318 infection to understand how the range expansion of three anuran species may have impacted the

319 course of their infection with *Batrachochytrium dendrobatidis*. We learned that at least one of

320 the anurans studied (*P. marmoratum*) is now using mountain passes cleared by the last 150 years

321 of deglaciation to disperse between watersheds separated by the Cordillera Vilcanota. We

322 learned that *Bd* is resilient to, and can disperse extensively at, even the highest elevations used by

323 amphibians. We also found evidence that some site infection metrics and sublethal impacts of

324 infection correlate with elevation, suggesting that this host range shift into new, high elevation

325 habitats has implications for infection outcomes.

326

327 **Genetic evidence suggests the recent introduction and extensive dispersal of**

328 ***Bd*GPL-2**

329

330 Whether global *Bd* epizootic events were provoked by a novel or endemic pathogen has not yet

331 been determined (Rachowicz et al. 2005, Rosenblum et al. 2013). We know that *Bd* was

332 frequently present in areas long before recorded epizootics (e.g. Soto-Azat et al. 2010, Rodríguez

333 et al. 2014, Becker et al. 2016, Adams et al. 2017, de León et al. 2019, Basanta et al. 2021).

334 Indeed, the earliest known *Bd* was swabbed from a Titicaca water frog (*Telmatobius culeus*)

335 collected in 1863, 300km southeast of the Cordillera Vilcanota (Burrowes and De la Riva

336 2017a). Scientists responsible for these pre-epizootic detections, and others across Amazonia

337 dating from 1895, propose that they represent endemic strains, and that regional *Bd*-associated

338 declines were driven by a novel strain invading in the 1990s (Becker et al. 2016, Burrowes and

339 De la Riva 2017a). The top candidate for this novel strain is the global panzootic lineage

340 (*Bd*GPL), the most derived *Bd* lineage in current phylogenies and the one most frequently

341 associated with chytridiomycosis. Despite occurring on every amphibian-inhabited continent

342 (Farrer et al. 2011, O'Hanlon et al. 2018), *Bd*GPL-2 shows little genetic structure (Schloegel et

343 al. 2012, James et al. 2015), suggesting its recent, rapid expansion (Farrer et al. 2011, Rosenblum

344 et al. 2013).

345

346   All *Bd* samples sequenced in this study belong to *Bd*GPL, consistent with previous studies

347   genotyping *Bd* collected from all South American sites west of the Brazilian Atlantic Forest

348   (O'Hanlon et al. 2018, Byrne et al. 2019, Russell et al. 2019, Alvarado-Rybak et al. 2021).

349   Additionally, *Bd* sampled from the Vilcanota was entirely from *Bd*GPL-2, the more derived and

350   globalized of two major proposed *Bd*GPL sub-clades (James et al. 2015). However, it is worth

351   noting that *Bd*GPL can outcompete older strains during coinfections, so may have displaced

352   potentially pre-existing endemic strains in the Vilcanota (Farrer et al. 2011, Jenkinson et al.

353   2018). Additionally, selecting the highest intensity swabs to sequence at each site could bias our

354   data against less-virulent strains (Farrer et al. 2011, Byrne et al. 2017).

355

356   We found Vilcanota *Bd*GPL-2 to be spatially unstructured using our genetic markers, consistent

357   with most previous genetic studies of *Bd*GPL, which have found it to be spatially unstructured

358   from local to continental scales (Velo-Antón et al. 2012, Byrne et al. 2019, Alvarado-Rybak et

359   al. 2021, Basanta et al. 2021, Rothstein et al. 2021). This lack of structure is generally interpreted

360   as evidence for its recent introduction to the areas sampled. One exception is the structured *Bd* of

361   the Sierra Nevada of California, suggesting the western U.S.A. as a potential origin for *Bd*GPL.

362   Sierran *Bd* demonstrates both that *Bd*GPL can develop spatial structure and that it can do so

363   despite cool, high-elevation conditions that may constrain rates of evolutionary change.

364

365   Although unstructured, Vilcanota *Bd*GPL-2 has substantial low-frequency variation,

366   representative of the global variation in *Bd*GPL-2. Our data cannot exclude the possibility that

367   *Bd*GPL circulated in the Vilcanota prior to the local epizootics of the early 2000s. However, in

368   the context of prior regional studies (Lips et al. 2008, Catenazzi et al. 2011, Burrowes et al.

369 2020), the most likely explanations are that *Bd*GPL-2 housed substantial standing genetic

370 variation upon its introduction or that it was introduced to the Vilcanota multiple times. Our

371 analyses place Vilcanota *Bd* in a large, global polytomy within *Bd*GPL-2. Therefore, we cannot

372 determine whether *Bd*GPL spread from Ecuador via the Andes (Lips et al. 2008) or from Brazil

373 via Bolivia (Catenazzi et al. 2011, Burrowes et al. 2020). However, the timing of *Bd*GPL-2's

374 arrival likely coincides with the onset of amphibian die-offs in the Vilcanota in the early 2000s

375 (Seimon et al. 2005, 2007), as this timing corresponds to declines in adjacent Amazonian and

376 cloud forest regions (Catenazzi et al. 2011).

377

378 Regardless of the provenance and timing of introduction, our data demonstrates that *Bd*GPL-2

379 has undergone extensive, frequent dispersal locally. It is clear the transmission of *Bd* across the

380 Cordillera Vilcanota was not limited to transmission by anurans along the terrestrial corridors

381 provided by deglaciated passes. Any process transporting moisture may have enabled its

382 dispersal*:* trade of *T. marmoratus* for urban consumption (Catenazzi et al. 2010), the introduction

383 and harvest of nonnative fish (Ortega and Hidalgo 2008, Martín-Torrijos et al. 2016), the

384 movements of Andean waterbirds (Burrowes and De la Riva 2017b), or even rainwater (Kolby et

385 al. 2015).

386

387 **Amphibians cannot escape *Bd* by range shifting upslope**

388

389 Early studies generally found that *Bd* infection prevalence or intensity increased with elevation

390 (Brem and Lips 2008) and that epizootics impacted highland sites more severely (Lips 1999,

391 Berger et al. 2004, Lips et al. 2006). These relationships are consistent with the preference of *Bd*

392 for cool temperatures (Piotrowski et al. 2004, Woodhams et al. 2008) and the impaired function

393 of the amphibian immune system and skin microbiome at colder, more thermally variable high

394 elevations (Jackson and Tinsley 2002, Daskin et al. 2014). Early field studies did not sample

395 above 2,500 m asl, but empirical work demonstrating that suboptimal temperatures retard *Bd*

396 growth led to a hypothesis that *Bd* pathogenicity was limited to elevations below 4,000 m asl

397 (Piotrowski et al. 2004, Ron 2005, Pounds et al. 2006, Woodhams et al. 2008). Subsequent

398 studies of amphibian communities up to 4,000 m asl reported declining *Bd* infection prevalence

399 or intensity with increasing elevation (Muths et al. 2008, Catenazzi et al. 2011), perhaps due as

400 much to increasing aridity as to decreasing temperatures at these higher elevations (De la Riva

401 and Burrowes 2011).

402

403 The idea that *Bd* pathogenicity had an upper elevational bound was undermined by the

404 documentation of severe infections above 4,000 m asl at several sites, including the Vilcanota

405 (Seimon et al. 2005, 2007, Knapp et al. 2011). From the data presented here, we find some

406 evidence that elevational extremes may constrain *Bd* growth. *Bd* infection metrics do appear to

407 decline at the upper reaches of the elevational gradient colonized by Vilcanota anurans (3,967—

408 5,333 m asl)—both for the significant and well-fit quadratic model of infection prevalence and

409 overall for the inherently noisy infection intensity data. Such declines would be consistent with

410 our expectations following from the temperature data recorded by our iButtons, considered in

411 light of a study profiling the thermal dependence of *Bd* growth (Voyles et al. 2017): we expect

412 *Bd* to experience lower average growth rates at higher elevations in the Vilcanota (Fig. 5).

413

414 **Upslope range shifts may mediate infection outcomes through exposure to**

415 **thermal variability**

416

417 We used body size and condition data to investigate whether extreme elevations compounded or

418 ameliorated the sublethal impacts of *Bd* infection. Amphibian body size and condition signal

419 important information about nutritional history, and can predict important fitness components

420 such as fecundity, the ability to respond effectively to environmental stress, and lifespan

421 (Martins et al. 2013, Brodeur et al. 2020).

422

423 At *Bd-* sites, *Telmatobius marmoratus* tadpole condition and size declined with increasing

424 elevations. *T. marmoratus* tadpoles have a protracted larval development relative to *P.*

425 *marmoratum* and *R. spinulosa*. During the estimated 5—19 months until metamorphosis

426 (Rodríguez-Papuico 1974, PNUD and ALT 2002, Lobos et al. 2018), they rely upon the

427 resources of their natal stream (Catenazzi et al. 2013a, Rubio 2019). Therefore, declines in

428 stream primary productivity with increasing elevation (Jacobsen 2008) might explain this trend

429 in tadpoles. A competing explanation could be that *T. marmoratus* tadpoles metamorphose more

430 quickly at increasing elevations, attaining a smaller size in the process (Licht 1975).

431

432 For larval *T. marmoratus*, circulating *Bd* was associated with decreased body condition and size

433 relative to developmental stage, but only at low elevations. This interaction is consistent with

434 expectations from our temperature data. Aquatic microhabitats at extreme elevations spend

435 significant amounts of time at no- or low-growth temperatures for *Bd*, resulting in a depressed

436 average growth rate, but at low elevation remain stably at temperatures conducive to *Bd* growth

437   (Fig. 5, Fig. S7). Studies of other amphibian species have shown that *Bd* infection can result in

438   smaller or lighter tadpoles (Parris and Cornelius 2004, Catenazzi et al. 2013b). Infected tadpoles

439   may sacrifice body size and condition by diverting energy towards immune response or by

440   accelerating metamorphosis (Warne et al. 2011). However, we expect that, for slow-developing

441   *T. marmoratus*, the impact of *Bd* on tadpole mouthparts is particularly important: *Bd* infects

442   keratinized tissues, which in tadpoles limits *Bd* growth to their mouthparts and causes oral

443   deformities over time (Berger et al. 1998, Vredenburg and Summers 2001), as has been

444   demonstrated for congenerics (Rubio 2019). Damaged mouthparts can reduce the efficiency of

445   tadpole feeding, reshape their feeding ecology, and retard their growth (Rowe et al. 1996,

446   Rachowicz and Vredenburg 2004, Rubio 2019).

447

448   Shared mechanisms may contribute to a similar trend in larval *P. marmoratum* body condition.

449   Their body condition declines with increasing elevations at *Bd*+ sites, but *Bd* infections appear to

450   take a larger energetic toll on *P. marmoratum* tadpoles at lower elevations. Larval *P.*

451   *marmoratum* differ from larval *T. marmoratus* in that the former increase in body size relative to

452   developmental stage with elevation, regardless of site infection status. This trend may reflect a

453   reproductive strategy that is advantageous under stressful, high elevation conditions: females

454   produce fewer offspring of higher quality in harsher environments. This strategy has been

455   documented in several anuran species (Lüddecke 2002, Räsänen et al. 2005, Liao et al. 2014).

456

457   Adult *P. marmoratum* body size also increases with elevation, perhaps owing to selection for

458   larger size at metamorphosis and larger females capable of greater maternal investment (Chen et

459   al. 2013, Liao et al. 2014, Womack and Bell 2020). However, their body size increases

460   dramatically with increasing elevation at *Bd*- sites, and only very gradually at *Bd*+ sites (6.5mm

461   vs. 1.4mm per 1,000m of elevation). In this case, *Bd* appears to have a larger sublethal toll at

462   higher elevations. While terrestrial animals experience lower average *Bd* growth rates at extreme

463   elevations, as animals inhabiting aquatic microhabitats, they are not as thermally buffered from

464   harsh temperature extremes. We found that adult *P. marmoratum* are more exposed to their

465   thermal tolerance limits at extreme high elevations (Fig. 5, Fig. S7), placing them at a fitness

466   disadvantage relative to the *Bd* pathogen (Cohen et al. 2017, 2019). Their failure to respond

467   phenotypically to high-elevation conditions could compromise their fecundity and survivorship,

468   and suggests that extreme elevations may compound rather than ameliorate the stress of *Bd*

469   infection for *P. marmoratum* adults.

470

471   **CONCLUSION**

472

473   Climate change will continue to drive range shifts, with many species expanding into colder and

474   more thermally-variable regions like the Vilcanota. It is important that we understand how the

475   stress of novel, frequently less optimal, habitats impacts host-pathogen systems, particularly in

476   the face of increasingly common emerging infectious disease challenges. In the case of

477   amphibian-*Bd* systems, hosts cannot escape this pathogen by range shifting upslope. *Bd* can

478   infect amphibians even at the edges of their physiological tolerances, although factors like

479   exposure to thermal variability may mediate infection outcomes. *Bd* has apparently undergone

480   frequent dispersal across the extreme elevation habitat of the Cordillera Vilcanota, with

481   transmission around this barrier not dependent on the formation of deglaciated dispersal

482 corridors. This work can help inform and stimulate further questions around how host range

483 shifts might in some cases exacerbate and in others mitigate emerging infectious disease events.

484

485 **REFERENCES**

486
487 Adams, A. J. et al. 2017. Extreme drought, host density, sex, and bullfrogs influence fungal pathogen

488   infection in a declining lotic amphibian. - Ecosphere 8: e01740.

489 Alvarado-Rybak et al. 2021. Chytridiomycosis outbreak in a Chilean giant frog (*Calyptocephalella gayi*)

490   captive breeding program: Genomic characterization and pathological findings. - Front. Vet. Sci. 8:

491   1–9.

492 Basanta, M. D. et al. 2021. Early presence of *Batrachochytrium dendrobatidis* in Mexico with a

493   contemporary dominance of the global panzootic lineage. - Mol. Ecol. 30: 424–437.

494 Becker, C. G. et al. 2016. Historical dynamics of *Batrachochytrium dendrobatidis* in Amazonia. -

495   Ecography. 39: 954–960.

496 Berger, L. et al. 1998. Chytridiomycosis causes amphibian mortality associated with population declines

497   in the rain forests of Australia and Central America. - Proc. Natl. Acad. Sci. 95: 9031–9036.

498 Berger, L. et al. 2004. Effect of season and temperature on mortality in amphibians due to

499   chytridiomycosis. - Aust. Vet. J. 82: 31–36.

500 Bosch, J. et al. 2007. Climate change and outbreaks of amphibian chytridiomycosis in a montane area of

501   Central Spain; is there a link? - Proc. R. Soc. B Biol. Sci. 274: 253–260.

502 Boyle, A.H.D. et al. 2007. Diagnostic assays and sampling protocols for the detection of

503   *Batrachochytrium dendrobatidis*. - Dis. Aquat. Organ. 73: 175–192.

504 Brem, F. M. R. and Lips, K. R. 2008. *Batrachochytrium dendrobatidis* infection patterns among

505   Panamanian amphibian species, habitats and elevations during epizootic and enzootic stages. - Dis.

506   Aquat. Organ. 81: 189–202.

507   Brodeur, J. C. et al. 2020. Frog body condition: Basic assumptions, comparison of methods and

508   characterization of natural variability with field data from *Leptodactylus latrans*. - Ecol. Indic. 112:

509   106098.

510   Burrowes, P. A. and De la Riva, I. 2017a. Unraveling the historical prevalence of the invasive chytrid

511   fungus in the Bolivian Andes: implications in recent amphibian declines. - Biol. Invasions 19: 1781–

512   1794.

513   Burrowes, P. and De la Riva, I. 2017b. Detection of the amphibian chytrid fungus *Batrachochytrium*

514   *dendrobatidis* in museum specimens of Andean aquatic birds: Implications for pathogen dispersal. -

515   J. Wildl. Dis. 53: 349–355.

516   Burrowes, P. A. et al. 2004. Potential causes for amphibian declines in Puerto Rico. - Herpetologica 60:

517   141–154.

518   Burrowes, P. A. et al. 2020. Genetic analysis of post-epizootic amphibian chytrid strains in Bolivia:

519   Adding a piece to the puzzle. - Transbound. Emerg. Dis. 67: 2163–2171.

520   Bustamante, M. R. et al. 2005. Cambios en la diversidad en siete comunidades de anuros en los Andes de

521   Ecuador. - Biotropica 37: 180–189.

522   Byrne, A. Q. et al. 2017. Unlocking the story in the swab: A new genotyping assay for the amphibian

523   chytrid fungus *Batrachochytrium dendrobatidis*. - Mol. Ecol. Resour. 17: 3218–3221.

524   Byrne, A. Q. et al. 2019. Cryptic diversity of a widespread global pathogen reveals expanded threats to

525   amphibian conservation. - Proc. Natl. Acad. Sci. 116: 20382–20387.

526   Catenazzi, A. et al. 2010. *Batrachochytrium dendrobatidis* in the live frog trade of Telmatobius (Anura :

527   Ceratophryidae) in the tropical Andes. - Dis. Aquat. Organ. 92: 187–191.

528   Catenazzi, A. et al. 2011. *Batrachochytrium dendrobatidis* and the collapse of anuran species richness and

529   abundance in the Upper Manu National Park, Southeastern Peru. - Conserv. Biol. 25: 382–391.

530   Catenazzi, A. et al. 2013a. Conservation of the high Andean frog *Telmatobius jelskii* along the PERU

531   LNG pipeline in the Regions of Ayacucho and Huancavelica, Peru. - In: Alonso, A. et al. (eds),

532   Monitoring biodiversity: Lessons from a Trans-Andean megaproject. Smithsonian Scholarly Press,

533   Washington, DC.

534   Catenazzi, A. et al. 2013b. High prevalence of infection in tadpoles increases vulnerability to fungal

535   pathogen in high-Andean amphibians. - Biol. Conserv. 159: 413–421.

536   Catenazzi, A. et al. 2017. Epizootic to enzootic transition of a fungal disease in tropical Andean frogs :

537   Are surviving species still susceptible? - PLoS One 12: e0186478.

538   Chen, W. et al. 2013. Maternal investment increases with altitude in a frog on the Tibetan Plateau. - J.

539   Evol. Biol. 26: 2710–2715.

540   Cohen, J. M. et al. 2017. The thermal mismatch hypothesis explains host susceptibility to an emerging

541   infectious disease. - Ecol. Lett. 20: 184–193.

542   Cohen, J. M. et al. 2019. An interaction between climate change and infectious disease drove widespread

543   amphibian declines. - Glob. Chang. Biol. 25: 927-937.

544   Daskin, J. H. et al. 2014. Cool temperatures reduce antifungal activity of symbiotic bacteria of threatened

545   amphibians - Implications for disease management and patterns of decline. - PLoS One 9: e100378.

546   De la Riva, I. and Burrowes, P. A. 2011. Rapid assessment of the presence of *Batrachochytrium*

547   *dendrobatidis* in bolivian Andean frogs. - Herpetol. Rev. 42: 372–375.

548   de León, M. E. et al. 2019. *Batrachochytrium dendrobatidis* infection in amphibians predates first known

549   epizootic in Costa Rica. - PLoS One 14: 1–14.

550   Edgar, R. C. 2004. MUSCLE: Multiple sequence alignment with high accuracy and high throughput. -

551   Nucleic Acids Res. 32: 1792–1797.

552   Enriquez-Urzelai, U. et al. 2019. Are amphibians tracking their climatic niches in response to climate

553   warming? A test with Iberian amphibians. - Clim. Change 154: 289–301.

554   Farrer, R. A. et al. 2011. Multiple emergences of genetically diverse amphibian infecting chytrids include

555   a globalized hypervirulent recombinant lineage. - PNAS 108: 1–6.

556   Fisher, M. C. et al. 2012. Emerging fungal threats to animal, plant and ecosystem health. - Nature 484: 1–

557   18.

558   Freeman, B. G. et al. 2018. Climate change causes upslope shifts and mountaintop extirpations in a

559   tropical bird community. - Proc. Natl. Acad. Sci. 115: 11982–11987.

560   Gosner, K. L. . 1960. A simplified table for staging anuran embryos and larvae with notes on

561   identification. - Herpetologica 16: 183–190.

562   Haddad, N. M. et al. 2014. Potential Negative Ecological Effects of Corridors. - Conserv. Biol. 28: 1178–

563   1187.

564   Harvell, C. D. et al. 2002. Climate warming and disease risks for yerrestrial and marine biota. - Science

565   (80-.). 296: 2158–2162.

566   Hoberg, E. P. and Brooks, D. R. 2015. Evolution in action: climate change, biodiversity dynamics and

567   emerging infectious disease. - Philos. Trans. R. Soc. B-Biological Sci. 370: 7.

568   Jackson, J. and Tinsley, R. 2002. Effects of environmental temperature on the susceptibility of *Xenopus*

569   *laevis* and *X. wittei* (Anura) to *Protopolystoma xenopodis* (Monogenea). - Parasitol. Res. 88: 632–

570   638.

571   Jacobsen, D. 2008. Tropical high-altitude streams. - In: Tropical Stream Ecology. Academic Press, pp.

572   219–256.

573   James, T. Y. et al. 2015. Disentangling host, pathogen, and environmental determinants of a recently

574   emerged wildlife disease: Lessons from the first 15 years of amphibian chytridiomycosis research. -

575   Ecol. Evol. 5: 4079–4097.

576   Jenkinson, T. S. et al. 2018. Globally invasive genotypes of the amphibian chytrid outcompete an

577   enzootic lineage in coinfections. - Proc. B 285: 20181894.

578   Jones, K. E. et al. 2008. Global trends in emerging infectious diseases. - Nature 451: 990–993.

579   Kamvar, Z. et al. 2014. Poppr: an R package for genetic analysis of populations with clonal, partially

580   clonal, and/or sexual reproduction. - PeerJ 2: e281.

581   Knapp, R. A. et al. 2011. Nowhere to hide: impact of a temperature-sensitive amphibian pathogen along

582   an elevation gradient in the temperate zone. - Ecosphere 2: 1–26.

583   Kolby, J. E. et al. 2015. Presence of amphibian chytrid fungus (*Batrachochytrium dendrobatidis*) in

584   rainwater suggests aerial dispersal is possible. - Aerobiologia (Bologna). 31: 411–419.

585   Korneliussen, T. S. et al. 2014. Open Access ANGSD : Analysis of Next Generation Sequencing Data. -

586   BMCBioinformatics 15: 356.

587   Lampo, M. et al. 2006. A chytridiomycosis epidemic and a severe dry season precede the disappearance

588   of Atelopus species from the Venezuelan Andes. - Herpetol. J. 16: 395–402.

589   Li, Y. et al. 2013. Review and synthesis of the effects of climate change on amphibians. - Integr. Zool. 8:

590   145–161.

591   Liang, L. and Gong, P. 2017. Climate change and human infectious diseases: A synthesis of research

592   findings from global and spatio-temporal perspectives. - Environ. Int. 103: 99–108.

593   Liao, W. B. et al. 2014. Altitudinal variation in maternal investment and trade-offs between egg size and

594   clutch size in the Andrew's toad. - J. Zool. 293: 84–91.

595   Licht, E. 1975. Comparative life history features of the western spotted frog, Ranapretiosa, from low- and

596   high-elevation populations. - Can. J. Zool. 53: 1254–1257.

597   Lips, K. R. 1999. Mass mortality and population declines of anurans at an upland site in Western Panama.

598   - Conserv. Biol. 13: 117–125.

599   Lips, K. R. et al. 2006. Emerging infectious disease and the loss of biodiversity in a Neotropical

600   amphibian community. - Proc. Natl. Acad. Sci. 103: 3165–3170.

601   Lips, K. R. et al. 2008. Riding the wave: Reconciling the roles of disease and climate change in

602   amphibian declines. - PLoS Biol. 6: 441–454.

603   Lobos, G. et al. 2018. Temporal gap between knowledge and conservation needs in high Andean

604   anurans : The case of the Ascotán salt flat frog in Chile. - South Am. J. Herpetol. 13: 33–43.

605   Lüddecke, H. 2002. Variation and trade-off in reproductive output of the Andean frog *Hyla labialis*. -

606   Oecologia 130: 403–410.

607   Martín-Torrijos, L. et al. 2016. Rainbow trout (*Oncorhynchus mykiss*) threaten Andean amphibians. -

608   Neotrop. Biodivers. 2: 26–36.

609   Martins, F. M. S. et al. 2013. Differential effects of dietary protein on early life-history and morphological

610   traits in natterjack toad (*Epidalea calamita*) tadpoles reared in captivity. - Zoo Biol. 32: 457–462.

611　Moritz, C. et al. 2008. Impact of a century of climate change on small-mammal communities in Yosemite

612　　　National Park, USA. - Science (80-.). 322: 261–264.

613　Muths, E. et al. 2008. Distribution and environmental limitations of an amphibian pathogen in the Rocky

614　　　Mountains, USA. - Biol. Conserv. 141: 1484–1492.

615　O'Hanlon, S. J. et al. 2018. Recent Asian origin of chytrid fungi causing global amphibian declines. -

616　　　Science (80-.). 360: 621–627.

617　Ortega, H. and Hidalgo, M. 2008. Freshwater fishes and aquatic habitats in Peru: Current knowledge and

618　　　conservation. - Aquat. Ecosyst. Heal. Manag. 11: 257–271.

619　Parmesan, C. et al. 1999. Poleward shifts in geographical ranges of butterfly species associated with

620　　　regional warming. - Nature 399: 579–583.

621　Parris, M. J. and Cornelius, T. O. 2004. Fungal pathogen causes competititve and developmental stress in

622　　　larval amphibian communities. - Ecology 85: 3385–3395.

623　Peig, J. and Green, A. J. 2009. New perspectives for estimating body condition from mass/length data:

624　　　The scaled mass index as an alternative method. - Oikos 118: 1883–1891.

625　Piotrowski, J. S. et al. 2004. Physiology of *Batrachochytrium dendrobatidis*, a Chytrid pathogen of

626　　　amphibians. - Mycologia 96: 9–15.

627　PNUD and ALT 2002. Evaluación de la población de la rana gigante del lago Titicaca Telmatobius

628　　　culeus. Crianza y manejo productivo de la rana gigante del lago Titicaca.

629　Poremba, R. J. et al. 2015. Meteorological Characteristics of Heavy Snowfall in the Cordillera Vilcanota ,

630　　　Peru. - 72nd East. Snow Conf.: 167–180.

631　Pounds, A. J. et al. 2006. Widespread amphibian extinctions from epidemic disease driven by global

632　　　warming. - Nature 439: 161–167.

633　Rachowicz, L. J. and Vredenburg, V. T. 2004. Transmission of *Batrachochytrium dendrobatidis* within

634　　　and between amphibian life stages. - Dis. Aquat. Organ. 61: 75–83.

635　Rachowicz, L. J. et al. 2005. The novel and endemic pathogen hypotheses : Competing explanations for

636　　　the origin of emerging infectious diseases of wildlife. - Conserv. Biol. 19: 1441–1448.

637 Raffel, T. R. et al. 2013. Disease and thermal acclimation in a more variable and unpredictable climate. -

638   Nat. Clim. Chang. 3: 146–151.

639 Räsänen, K. et al. 2005. Maternal investment in egg size: Environment- and population-specific effects on

640   offspring performance. - Oecologia 142: 546–553.

641 Raxworthy, C. J. et al. 2008. Extinction vulnerability of tropical montane endemism from warming and

642   upslope displacement: A preliminary appraisal for the highest massif in Madagascar. - Glob. Chang.

643   Biol. 14: 1703–1720.

644 Reider, K. E. 2018. Survival at the summits : Amphibian responses to thermal extremes, disease, and

645   rapid climate change in the high tropical Andes by. – PhD thesis, Florida International University,

646   USA.

647 Reider, K. E. et al. 2020. Thermal adaptations to extreme freeze–thaw cycles in the high tropical Andes. -

648   Biotropica 53: 296–306.

649 Rodríguez-Papuico, H. 1974. Experimentos sobre adaptación, crianza y procesamiento de la rana de

650   Junín. –PhD thesis, Universidad Nacional Agradia La Molina, Peru.

651 Rodríguez, D. et al. 2014. Long-term endemism of two highly divergent lineages of the amphibian-killing

652   fungus in the Atlantic Forest of Brazil. - Mol. Ecol. 23: 774–787.

653 Rohr, J. R. and Raffel, T. R. 2010. Linking global climate and temperature variability to widespread

654   amphibian declines putatively caused by disease. - Proc. Natl. Acad. Sci. 107: 8269–8274.

655 Ron, S. R. 2005. Predicting the distribution of the amphibian pathogen *Batrachochytrium dendrobatidis*

656   in the new world. - Biotropica 37: 209–221.

657 Rosenblum, E. B. et al. 2013. Complex history of the amphibian-killing chytrid fungus revealed with

658   genome resequencing data. - Proc. Natl. Acad. Sci. 110: 9385–9390.

659 Rothstein, A. P. et al. 2021. Divergent regional evolutionary histories of a devastating global amphibian

660   pathogen. - Proceeding 288: 20210782.

661 Rowe, C. L. et al. 1996. Oral deformities in tadpoles (*Rana catesbeiana*) associated with coal ash

662   deposition: effects on grazing ability and growth. - Freshw. Biol. 36: 727–730.

663   Rubio, A. O. 2019. Effects of the fungal pathogen *Batrachochytrium dendrobatidis* on the trophic

664   ecology of tadpoles of Andean water frogs. –MS thesis, Southern Illinois University Carbondale,

665   USA.

666   Russell, I. D. et al. 2019. Widespread chytrid infection across frogs in the Peruvian Amazon suggests

667   critical role for low elevation in pathogen spread and persistence. - PLoS One 14: e0222718.

668   Scheele, B. C. et al. 2019. Amphibian fungal panzootic causes catastrophic and ongoing loss of

669   biodiversity. - Science (80-.). 1463: 1459–1463.

670   Schloegel, L. M. et al. 2012. Novel, panzootic and hybrid genotypes of amphibian chytridiomycosis

671   associated with the bullfrog trade. - Mol. Ecol. 21: 5162–5177.

672   Schmidt, S. K. et al. 2009. Microbial activity and diversity during extreme freeze – thaw cycles in

673   periglacial soils, 5400 m elevation, Cordillera Vilcanota, Peru. - Extremophiles 13: 807–816.

674   Seimon, T. A. et al. 2005. Identification of chytridiomycosis in *Telmatobius marmoratus* at 4450 m in the

675   Cordillera Vilcanota of southern Peru. - Monogr. Herpetol. 7: 275–283.

676   Seimon, T. A. et al. 2007. Upward range extension of Andean anurans and chytridiomycosis to extreme

677   elevations in response to tropical deglaciation. - Glob. Chang. Biol. 13: 288–299.

678   Seimon, T. A. et al. 2017. Long-term monitoring of tropical alpine habitat change, Andean anurans, and

679   chytrid fungus in the Cordillera Vilcanota, Peru: Results from a decade of study. - Ecol. Evol. 7:

680   1527–1540.

681   Skerratt, L. F. et al. 2007. Spread of chytridiomycosis has caused the rapid global decline and extinction

682   of frogs. - Ecohealth 4: 125–134.

683   Soto-Azat, C. et al. 2010. Widespread historical presence of *Batrachochytrium dendrobatidis* in African

684   pipid frogs. - Divers. Distrib. 16: 126–131.

685   Velo-Antón, G. et al. 2012. Amphibian-killing fungus loses genetic diversity as it spreads across the New

686   World. - Biol. Conserv. 146: 213–218.

687   Voyles, J. et al. 2017. Diversity in growth patterns among strains of the lethal fungal pathogen

688   *Batrachochytrium dendrobatidis* across extended thermal optima. - Oecologia 184: 363–373.

689 Vredenburg, V. T. and Summers, A. P. 2001. Field identification of chytridiomycosis in *Rana muscosa*

690   (Camp 1915). - Herpetol. Rev. 32: 151–152.

691 Wang, Q.-W. et al. 2014. Is UV-induced DNA damage greater at higher elevation? - Am. J. Bot. 101:

692   796–802.

693 Warne, R. W. et al. 2011. Escape from the pond: Stress and developmental responses to ranavirus

694   infection in wood frog tadpoles. - Funct. Ecol. 25: 139–146.

695 Womack, M. C. and Bell, R. C. 2020. Two-hundred million years of anuran body-size evolution in

696   relation to geography, ecology and life history. - J. Evol. Biol. 33: 1417–1432.

697 Woodhams, D. C. et al. 2008. Life-history trade-offs influence disease in changing climates: Strategies of

698   an amphibian pathogen. - Ecology 89: 1627–1639.

699

700

701

702

703

704 **FIGURES**
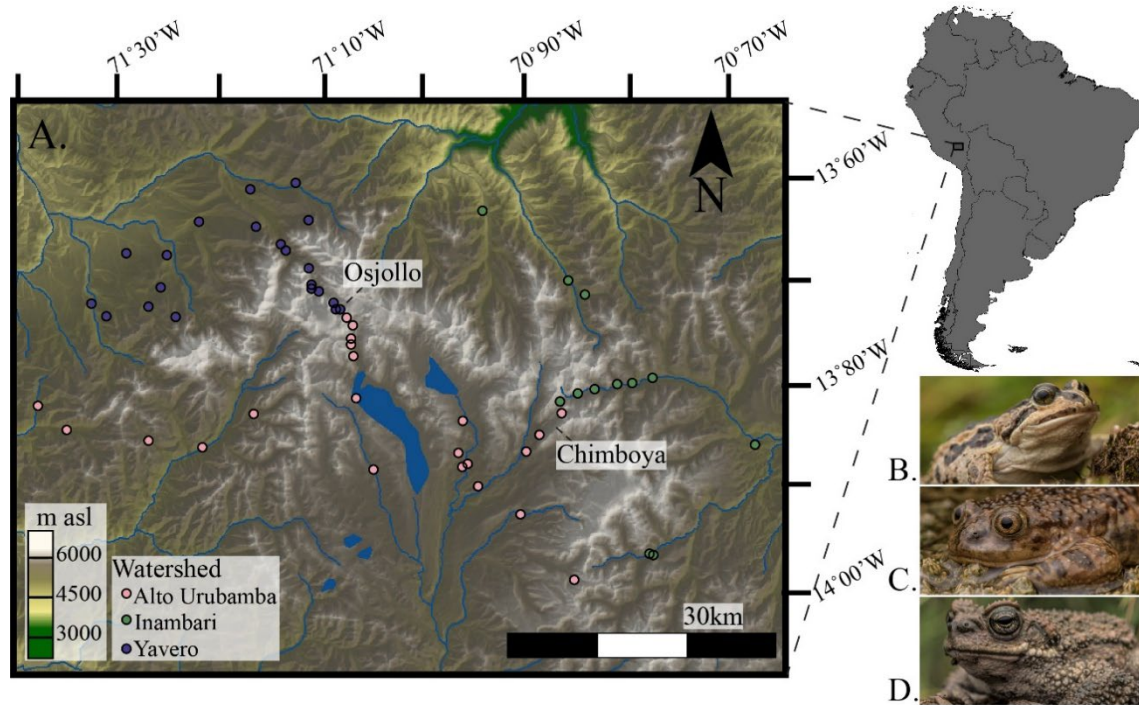
Figure 1. The study system. **(A)** Sites where amphibians and *Batrachochytrium dendrobatidis* were sampled in the Cordillera Vilcanota, colored to represent their watershed location and plotted over a hillshaded digital elevation model (DEM). The two deglaciated mountain passes, Osjollo and Chimboya, are labeled. The study species **(B)** *Pleurodema marmoratum*, **(C)** *Telmatobius marmoratus*, and **(D)** *Rhinella spinulosa* are also pictured. Photos courtesy of Anton Sorokin.
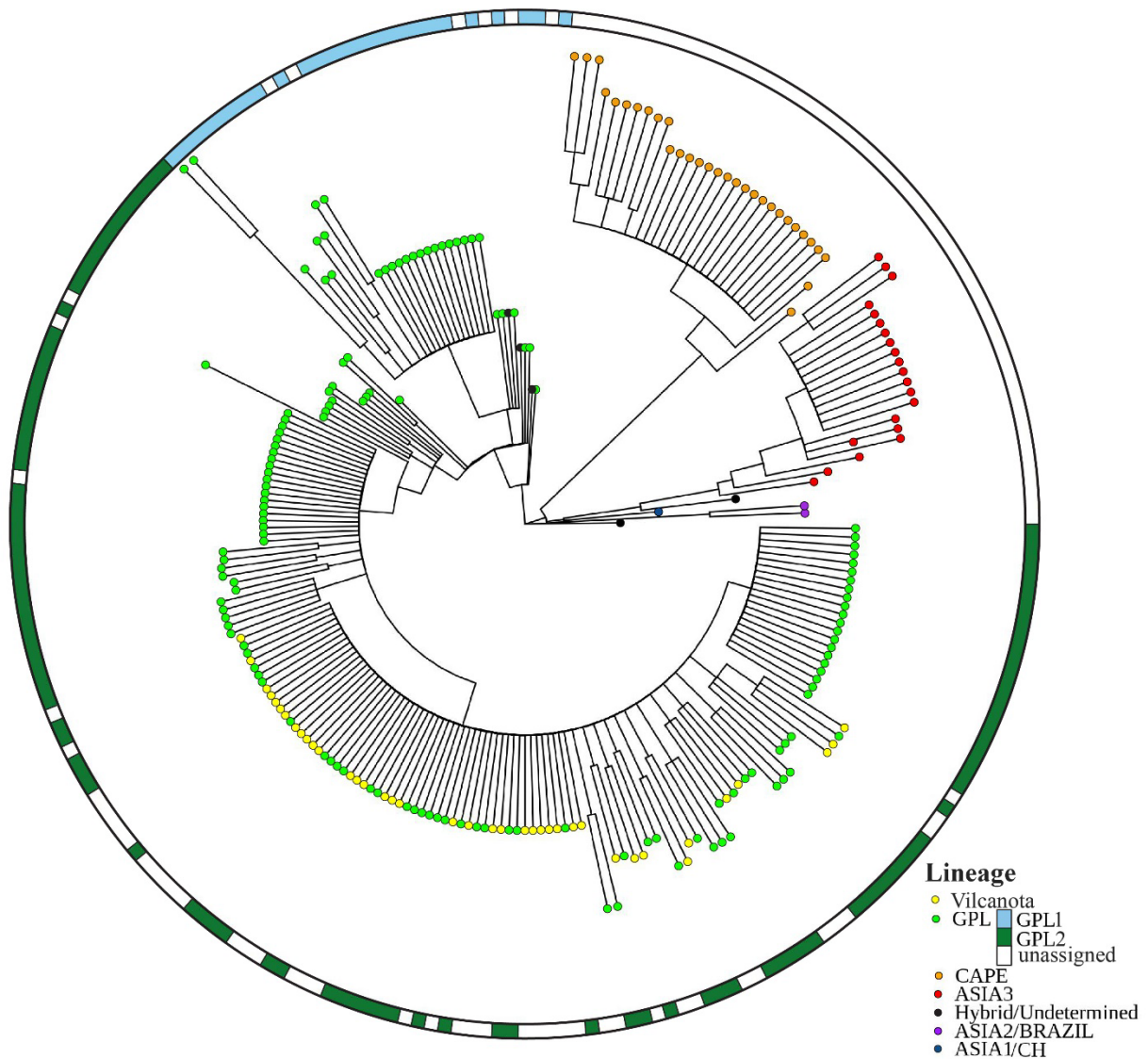
Figure 2. A midpoint-rooted consensus gene tree of Vilcanota Bd sampled from *Pleurodema marmoratum* (yellow tips) alongside previously-published samples representative of the five major *Bd* lineages (CAPE, ASIA3, ASIA2/BRAZIL, ASIA1/CH, GPL) and their hybrids (2). This tree has a normalized quartet score of 0.807 and includes only nodes with a posterior probability ≥0.7. Assignment of *Bd*GPL samples to *Bd*GPL-1 or *Bd*GPL-2 is based on previous studies (3–5) and is shown in the concentric mosaic. This tree is included with sample names and the continent of swab origin in the supplements (Figure S 1).
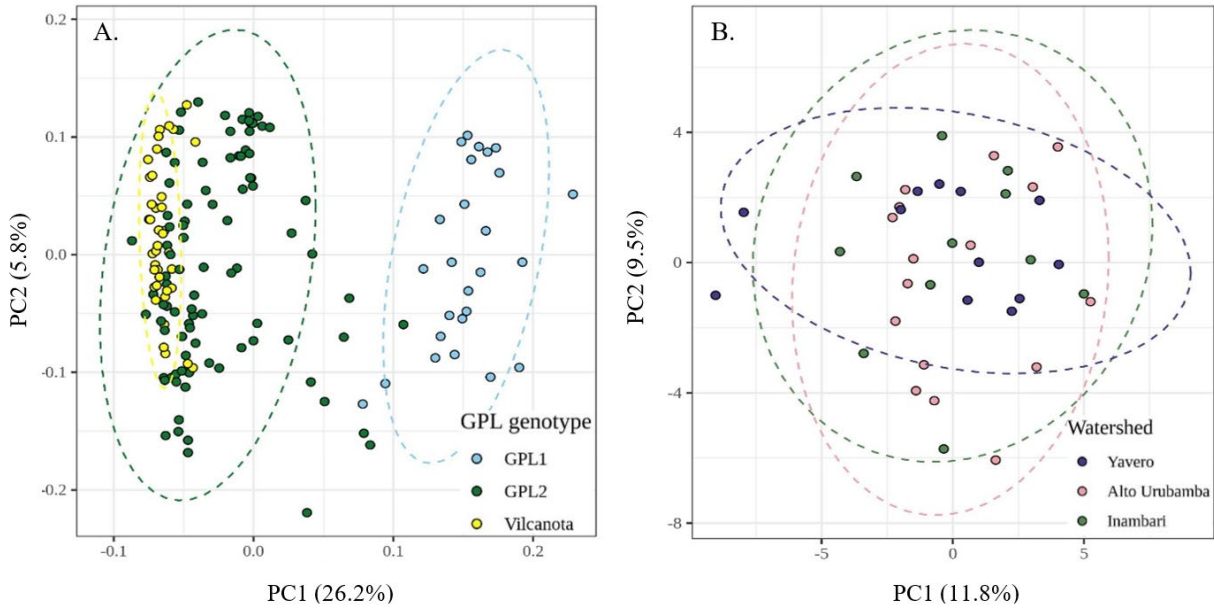
711

712

713

714

715

716

Figure 3. Principal component analyses (PCAs) of **(A)** global *Bd*GPL samples, demonstrating how *Bd* sampled from *Pleurodema marmoratum* in the Vilcanota is nested within the *Bd*GPL-2, and **(B)** Vilcanota samples, colored by watershed, showing their lack of genetic structure.
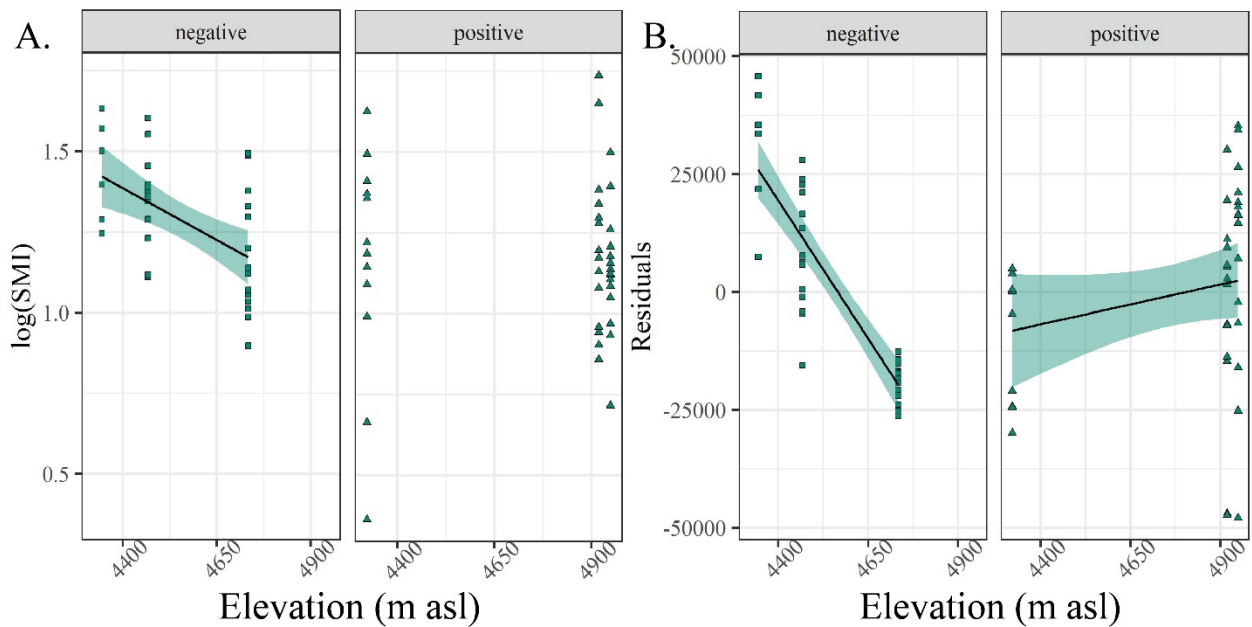

Figure 4. The sublethal impacts of *Bd* exposure on *T. marmoratus* tadpoles. **(A)** Linear mixed model of *T. marmoratus* tadpole body condition (SMI) along the elevational gradient, displayed in separate panels for *Bd*-positive and *Bd*-negative sites. **(B)** Linear mixed model of *T. marmoratus* tadpole residuals of body size (SVL) against Gosner stage, displayed in separate panels for *Bd*-positive and *Bd*-negative sites. These trends cannot be attributed to systematic differences in the timing of sampling (Fig S 6D).
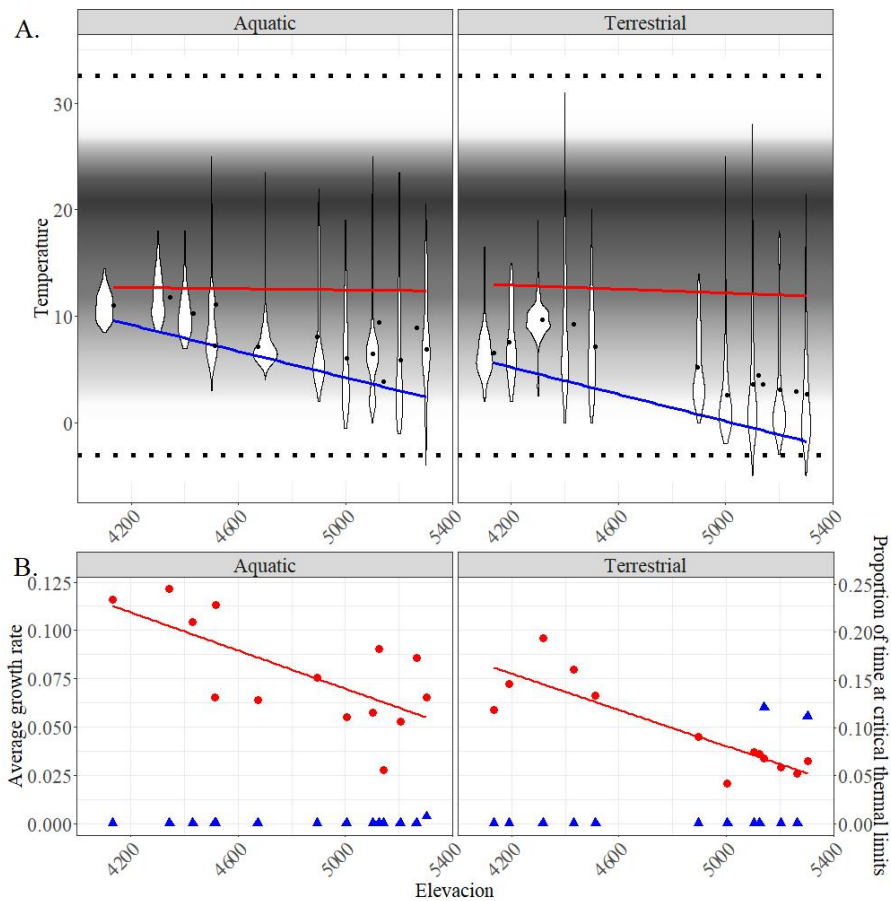
Figure 5. Thermal regimes along the elevational gradient and across microhabitats. **(A)** Violin plots of raw temperature data. Mean daily temperatures measured by a given iButton are displayed as black points. The red and blue lines represents linear regression of maximal and minimal daily temperatures, respectively. The black gradient represents the logistic growth rate (r) of a tropical *Bd* strain quantified across temperatures by Voyles et al. 2017. The upper black dotted line represents the CT_{max} of adult *P. marmoratum* (32.56˚C), and the lower dotted line represents the mean temperature tolerated by *P. marmoratum* adults that recovered following freezing (Reider et al 2020). **(B)** Red points represent the average growth rate of *Bd* according to the temperatures recorded by a given iButton, and the red line represents a linear regression of this data. Blue triangles represent the proportion of time a given iButton was exposed to temperatures outside the physiological tolerance of *P. marmoratum* adults.